Optics and Lasers in Engineering 176 (2024) 108088

Contents lists available at ScienceDirect

Optics and Lasers in Engineering

journal homepage: www.elsevier.com/locate/optlaseng

From 3D to 5D: Computational light-in-flight imaging via an SPAD camera

Zhi-Guan Wang [a,b], Ming-Jie Sun [a,*], Daniele Faccio [c]

[a] School of Instrumentation and Optoelectronic Engineering, Beihang University, Beijing 100191, China
[b] Shenyuan Honors College, Beihang University, Beijing 100191, China
[c] School of Physics and Astronomy, University of Glasgow, Glasgow G128QQ, UK

ARTICLE INFO

Keywords:
Light-in-flight imaging
Single-photon avalanche diode camera
Ultrafast imaging

ABSTRACT

Light-in-flight imaging, which images light itself at high frame rates, is an intuitive method for studying light-related ultrafast phenomena. Usually, light propagation happens in five dimensions, i.e. (x, y, z, t, n) if the refractive index of the medium is unknown. However, state-of-art imaging devices, such as single-photon avalanche diode cameras, capture only three-dimensional (x', y', t') data, which are merely the projection of the five-dimensional information on the light-sensitive detector array. The recovery of the five-dimensional information from its three-dimensional projection is an intrinsically ill-posed problem. By considering the continuous nature of light propagation, this work demonstrates that it is possible to retrieve the five-dimensional information from the captured data of a single-photon avalanche diode camera. The feasibility of the proposed method is verified in different scenarios, including light propagating in a uniform medium, travelling along curved optical fibers, and bending in a gradient refractive index medium, with an averaged reconstruction accuracy of about 1 %. The proposed method broadens the applicable scope of light-in-flight imaging and provides insights for high-dimensional information retrieval.

1. Introduction

Light-in-flight (LiF) imaging can freeze light in motion and provides fundamental information for studying light transport phenomena and applications such as looking around corners or imaging through scattering media [1–4]. Three-dimensional LiF imaging that records the (x', y', t') information of propagating light was first demonstrated by holography in 1978 [5] and recently by the white light interferometer [6–8] with higher temporal resolution. In the past few years, imaging devices with single-photon sensitivity and high temporal resolution have emerged. Using those imaging devices, such as streak cameras [9], photonic mixer devices (PMD) [10], and single-photon avalanche diode (SPAD) cameras [11], 3D LiF imaging of light traveling through static scenes, propagating in optical fibers [12], and being reflected by mirrors [13] was achieved by detecting the scattered photons from the flying light.

Although existing imaging devices can directly obtain the 3D information of light, one may neglect that light propagates in four-dimensional (x, y, z, t) space-time. If the refractive index is unknown, light propagation is related to five-dimensional (x, y, z, t, n) information. The 3D (x', y', t') data captured by the imaging devices are merely the low-dimensional projection of the 5D information on the light-sensitive detector array. The 5D information, which contains the 4D LiF information and the medium's refractive index, is essential for studying light propagation. However, retrieving the 5D information from the 3D data is an intrinsically ill-posed problem.

Typically, we need additional constraints on the solution space to obtain a solution to an ill-posed problem. For example, under the constraint that light freely propagates in air, the extra depth information of light can be retrieved from the 3D data. Laurenzis *et al.* demonstrated calculating the propagation angles of straight light paths in air via an SPAD camera [14]. Subsequently, Zheng *et al.* recognized that when light travels in air along straight paths, the projection from the 4D (x, y, z, t) LiF information to the 3D (x', y', t') SPAD data is a one-to-one mapping. Therefore, the 4D LiF information was retrieved via a computational layer, and the spatiotemporal distortion induced by the relativistic effect was corrected [15]. Subsequently, the 4D LiF imaging with corrected intensity [16] and the megapixel 4D LiF imaging [17] were demonstrated based on the same principle.

State-of-art 4D LiF imaging methods are feasible under the condition of straight light paths and a known refractive index. However, in many scenarios, such as light propagating in a waveguide, the shape of the

* Corresponding author.
E-mail address: mingjie.sun@buaa.edu.cn (M.-J. Sun).

https://doi.org/10.1016/j.optlaseng.2024.108088
Received 17 November 2023; Accepted 28 January 2024

light path and the refractive index are unknown. Retrieving the 5D information in these scenarios is an ill-posed problem and has yet to be explored.

We notice that light paths are continuous in most scenarios of light propagation, which provides constraints for the ill-posed problem. Based on this insight, we propose a LiF imaging method that can retrieve the 5D information (i.e., the 4D LiF information and the refractive index distribution of the medium) via an SPAD camera. To achieve this, we first build a general optical model to map the 5D information to the 3D data of the SPAD camera. Subsequently, by utilizing the continuous nature of light paths, we formulate an optimization problem to retrieve the 5D information from the 3D data. We validate the feasibility of the method in scenarios including light propagating in a uniform medium, in optical fibers, and in a gradient refractive index (GRIN) medium.

2. Method

2.1. General optical model

Light propagation occurs in real space, and the 5D (x, y, z, t, n) information is defined in the world coordinate system. However, when capturing the light propagation by a SPAD camera, the captured (x', y') data are presented in the pixel coordinate system. Besides, the time t' is recorded by the time-to-digital converter (TDC) of the SPAD pixel, which is the sum of the original propagation time t of the light and the scattering time t_s during which the scattered photons propagate from the spatial location of the light to that of the SPAD camera. Here, we develop a general optical model to transform the 5D (x, y, z, t, n) information in real space to the (x', y', t') 3D data captured by the SPAD camera.

We build the general optical model based on two assumptions:

Assumption 1. We regard the SPAD camera as a pinhole camera and treat the SPAD pixels as discrete points. According to the pinhole camera model, only the scattered photons from some discrete object points on the light path can pass through the aperture and hit the SPAD pixels. Hence, there is a one-to-one mapping between the object points in real space (x, y, z) and the SPAD pixels presented in the pixel coordinate system (x', y').

Assumption 2. Generally speaking, a medium's refractive index distribution is a function relating to (x, y, z). When light enters a medium, the light path bends in the x- and y-direction due to the index variation along the corresponding directions. The curved light path can be recorded by the SPAD camera, and it is possible to retrieve the refractive index profile by processing the captured image [18,19]. However, the refractive index variation along the z-axis will bend the light path in the z-direction, which cannot be captured by the camera. Hence, it is more difficult to retrieve the refractive index profile along the z-axis. The model presented here will focus on this challenging situation, and we assume that the refractive index of the medium changes only along the z-axis.

Since the 3D data recorded by the SPAD camera are discrete, we discretize the 5D information in real space by introducing two approximations:

Approximation 1. In mathematics, when closely observing a general function, we can represent it using a linear function. We also apply the linear approximation to the light path. As the object points are densely distributed on the light path, we approximate the light paths between any two adjacent object points as straight lines. Therefore, we can use these object points to discretely represent the whole light path.

Approximation 2. The whole medium is regarded as a cube that contains all the object points on the light path. We segment the medium into multiple layers along the z-axis, with the object points as the demarcations. As the refractive index change is relatively small within each layer, we approximate that each layer is homogeneous, and the refractive index profile is converted into discrete values.

Based on these two approximations, the 5D information is discretized into the 4D (x, y, z, t) LiF information at the object points and the refractive indices of all the layers. The pixel number of the SPAD camera determines the maximum number of the object points and the layers.

Fig. 1 depicts the schematic diagram of the general optical model for mapping the discrete 5D information to the 3D data. There are m object points on the light path, denoted as O_i ($i = 1, 2, \ldots, m$). The straight-line length between O_i and O_{i+1} is denoted as l_i. The medium is divided into (m-1) layers, and n_j ($j = 1, 2, \ldots, m$-1) represents the refractive index of each layer. We define the moment when light reaches O_1 as the time zero.

The scattering paths indicate how the scattered photons travel from the object points to the corresponding pixels. Please note that the scattering paths are curved due to refraction, but their segments within each layer are approximately straight. For a scattering path originating from O_i, $s_{i,j}$ represents the length of its segment within layer j, while d_i denotes the length of its segment outside the medium.

As SPAD cameras typically work under dry conditions, we consider the ambient medium to be air with a refractive index of 1. However, the ambient medium can theoretically be any transparent substance, such as glass or water.

According to the general optical model, we can transform the discrete 5D information into the 3D data in two steps:

Step1. Calculation of the (x', y') data from the discrete (x, y, z, n) information. Starting from each object point, we trace the scattering paths according to Snell's law. The scattering paths traverse all medium layers and the optical center of the SPAD camera, finally reaching the corresponding pixel. Consequently, we acquire the (x', y') data.

Step2. Calculation of the measured time t'_i at each object points. We can divide t'_i into two parts:

$$t'_i = t_i + t_{si}, i = 2, 3, \ldots, m, \tag{1}$$

where t_i denotes the light propagation time from O_1 to O_i, and t_{si} is the scattering time of the photons from O_i to the camera. Although t_i is a

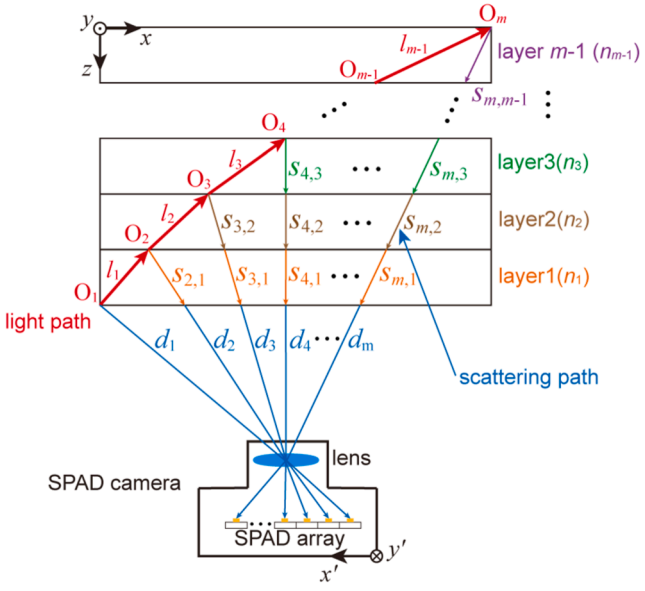

Fig. 1. The general optical model for converting the 5D information to the 3D data. The object points on the light path are denoted as O_i ($i = 1, 2, \ldots, m$). The light path segments between two adjacent object points are approximated as straight lines, and the straight-line length between O_i and O_{i+1} is represented by l_i. Using the object points as demarcations, the cubic medium is divided into (m-1) layers along the z-axis, and n_j ($j = 1, 2, \ldots, m$-1) represents the refractive index of each layer. It should be noted that the scattering paths are curved, but their segments within each layer are approximately straight. For a scattering path originating from O_i, $s_{i,j}$ denotes the length of its segment within layer j, while d_i represents the length of its segments outside the medium. We assume the ambient medium is air.

known value, we can also represent t_i by $t_{i\text{-}1}$:

$$t_i = t_{i-1} + \frac{n_L l_{i-1}}{c}. \tag{2}$$

The second term of Eq. (2) computes the propagation time from $O_{i\text{-}1}$ to O_i, and $l_{i\text{-}1}$ is the distance between these two points. n_L denotes the refractive index along the light path. When the light propagates in a waveguide, n_L is the refractive index of the waveguide. If the light travels freely within the medium, n_L equals $n_{i\text{-}1}$. Besides, t_{si} can be calculated:

$$t_{si} = \frac{\sum_{j=1:i-1} n_j s_{i,j} + d_i}{c}, \tag{3}$$

where $s_{i,j}$ and d_i are determined during the process of tracing the scattering paths from the object points to the SPAD pixels.

Eq. (2) illustrates the correlation between the propagation times at adjacent object points. The propagation time t_1 at the first object point O_1 is zero, and we can sequentially calculate the propagation times at O_2 - O_m according to Eq. (2). Therefore, the 5D (x, y, z, t, n) information is equivalent to the 4D (x, y, z, n) information, allowing us to use only the 4D (x, y, z, n) information to obtain the 3D data in the camera space.

Based on the general optical model, we can develop specific forward models for transforming the 4D information into the 3D data in various scenarios of light propagation. Here, we demonstrate the forward models in three typical scenarios: light propagates freely in a homogeneous medium, light travels in an optical waveguide, and light bends in a GRIN medium. We also investigate the inverse problems in these three scenarios.

Scenario 1: Light propagates freely in a homogeneous medium. The refractive index of the homogeneous medium is demoted by n, and the refractive indices of all the layers are the same. The refraction of the scattered photons only exists in the medium-air interface. We can convert the 3D (x, y, z) position of the object points into the 2D (x', y') pixel position by tracing the scattering path. The forward model to calculate t' is:

$$t_i' = t_{i-1} + \frac{n l_{i-1}}{c} + \frac{n s_i + d_i}{c}, i = 2, 3, \ldots, m. \tag{4}$$

Due to the homogeneity of the medium, the scattering path within the medium is a straight line, and the sum of $s_{i,j}$ in Eq. (3) is denoted by a single variable s_i in Eq. (4), representing the total length of the scattering path from S_i to the medium-air interface. We consider the inverse problem, which aims to determine the 4D (x, y, z, n) information in real space from the 3D (x', y', t') data. We assume that the position of O_1 is known and try to determine the position of O_2 and n based on the forward model. d_2 can be determined by (x'_2, y'_2) and the depth of O_1, and there are three unknown variables in Eq. (4): n, s_2, and l_1. We can calculate s_2 and l_1 by the position of O_2. However, even if we consider that O_2 is on the scattering path corresponding to the pixel at (x'_2, y'_2), we still need its depth to determine its position. Consequently, the inverse problem is ill-posed as only one equation is available, while the depth of O_2 and n are unknown.

Scenario 2: Light travels in an optical waveguide. We assume the waveguide is situated in air. Since there is no refraction along the scattering paths, we can convert the (x, y, z) information to the (x', y') data by the internal matrix of the SPAD camera. Furthermore, in Eq. (3), n_j equals the refractive index of air, and the summation of $s_{i,j}$ can be represented as s_i. In this scenario, t' can be calculated by:

$$t_i' = t_{i-1} + \frac{n_w l_{i-1}}{c} + \frac{s_i + d_i}{c}, i = 2, 3, \ldots, m, \tag{5}$$

where n_w is the refractive index of the waveguide. Similar to that in scenario 1, the inverse problem here to calculate the position of O_2 by (x'_2, y'_2, t'_2) is ill-posed as both the depth of O_2 and n_w are unknown.

Scenario 3: Light bends in a GRIN medium. We can calculate the (x', y') data from the (x, y, z) information by tracing the scattering paths, during which we must consider multiple refractions as the refractive index of each layer is different. The forward model to calculate t' is:

$$\begin{aligned} t_i' &= t_{i-1} + \frac{n_{i-1} l_{i-1}}{c} + \frac{\sum_{j=1:i-1} n_j s_{i,j} + d_i}{c}, \\ i &= 2, 3, \ldots, m, \end{aligned} \tag{6}$$

where $s_{i,j}$ and d_i are determined while tracing the scattering path. The inverse problem associated with Eq. (6) is also ill-posed since both $l_{i\text{-}1}$, $s_{i,j}$, and n_j ($j = 1, \ldots, i\text{-}1$) are unknown when calculating the position of an object point O_i.

2.2. Retrieval algorithm

As demonstrated in Section 2.1, retrieving the 5D information from the 3D data is an ill-posed problem. Additionally, the temporal noise from the SPAD camera further hinders accurate reconstruction. Nevertheless, compressed sensing demonstrates that, by exploiting the sparsity of a signal, the ill-posed problem of reconstructing a signal from a limited number of samples can be solved [20]. Therefore, we can solve the ill-posed problem of retrieving the 5D information by using proper prior information about light paths.

We focus on the geometric characteristics of light paths. In general, light paths are continuous until all photons are absorbed. When light propagates in a homogeneous medium, in a waveguide, or in a GRIN medium, the light paths are smooth. If further considering that the direction of light changes dramatically due to reflection or refraction, the light paths are piecewise smooth. In summary, the continuous light paths are smooth or piecewise smooth, and this characteristic can serve as prior information to retrieve the 5D information.

The smoothness of a curve can be mathematically quantified by integrating its squared second derivative [21], and a smaller integral corresponds to a smoother curve. As we have discretized the light path, we apply the second-order differencing to K ($K = \{k_1, k_2, k_3 \ldots\}$), which represents the slopes of the straight path segments, to quantify its smoothness. We induce the prior information of smoothness by minimizing either the L_1 norm or the L_2 norm of $\Delta^2 K$. Therefore, an optimization problem is formulated:

$$\begin{aligned} &[K^*, N^*] = \arg\min_{K,N} \| \Delta^2 K \|_{p,p\in\{1,2\}} \\ &s.t. \| f(K,N) - T' \|_2 \le \sqrt{m\sigma^2}. \end{aligned} \tag{7}$$

The first term is the objective function, and the second term is the data fidelity term, which maintains the light path within the valid solution space throughout the iteration process. N ($N = \{n_1, n_2, \ldots, n_{m\text{-}1}\}$) are the refractive indices of all the layers, while T' ($T' = \{t'_1, t'_2, \ldots, t'_m\}$) are the temporal data measured by the SPAD camera. Based on K, the 2D (x', y') data, and the known position of O_1, we can sequentially compute the 3D positions of the sample points, and then we can calculate t' by the 4D (x, y, z, n) information based on the forward models presented in Section 2.1. $f(K, N)$ denotes the operator for computing t'. We use σ to denote the standard deviation of the temporal noise, which is determined during camera calibration. We use random numbers to initialize K and N.

Solving this optimization problem yields K^* representing a smooth light path and the corresponding N^*. Afterward, by calculating the positions of the object points using K^*, we obtain the (x, y, z) information. Next, the temporal information t can be calculated from the (x, y, z, n) information by Eq. (2), and we obtain the 5D information. In cases where the light path is piecewise smooth, we can retrieve each smooth segment and connect them.

3. Results

3.1. Result of light propagating along straight paths

To test the proposed method in a homogeneous medium, we perform an experiment to reconstruct the 5D information when light reflects between two mirrors in air. In our reconstruction, we consider the refractive index of air as an unknown value to demonstrate the method's capability to reconstruct the refractive index. The light propagates in a 375 × 75 × 50 mm 3D space, and the (x', y', t') data are captured by an SPAD camera (Photon Force PF32). The detailed experiment setup and the data processing are provided in Section 3.2. There are two singular points on the continuous light path due to reflections. Therefore, we treat the whole path as a combination of three straight paths and reconstruct each straight path independently, and then we connect these straight paths to reconstruct the whole path.

The 5D imaging result is depicted in Fig. 2. The root mean square errors (RMSEs) in position and time are 5.01 mm and 9.37 ps. The measured refractive index of air is 1.000, while the ground truth under laboratory conditions is 1.00027 (@λ = 633 nm, 293 K, 1 atm, 25 % humidity [22]).

3.2. Results of light propagating in curved optical fibers

Optical fibers are the most used among various types of waveguides. Therefore, this study primarily investigates the scenario of light traveling in optical fibers. First, we present a simulation of 5D imaging when light propagates in curved optical fibers. The projection of the simulated curved optical fiber onto the x-z plane forms a sinusoidal curve, while its projection onto the x-y plane is a parabola. The simulated spatial resolution of the SPAD camera is 32 × 32, and the object distance is 370 mm, where the field of view (FOV) is 140 mm × 140 mm. There are 32 object points on the simulated light path. We also add random temporal noise to the synthetical temporal data.

In this simulation, we test different objective functions of the optimization problem in Section 2.2. The imaging result obtained by optimizing $||\Delta^2 K||_1$ is shown in Fig. 3(a), achieving RMSEs of 2.62 mm and 8.24 ps in position and time, respectively. The reconstructed refractive index of the optical fiber is 1.445, while the ground truth is 1.450. Since the L_1 norm preserves sparse elements with large values while suppressing small elements, the overall shape of the light path is retained, but some details are lost. Next, we reconstruct the light propagation by optimizing $||\Delta^2 K||_2$, resulting in RMSEs of 8.20 mm and 25.56 ps, as shown in Fig. 3(b). The reconstructed refractive index is 1.404. The reconstruction is worse since the L_2 norm equally suppresses all elements, resulting in a small and uniform sequence of $\Delta^2 K$, which cannot represent light paths with significant curvature changes.

Additionally, we introduce a joint objective function [23,24] that combines $||\Delta^2 K||_1$ and $||\Delta^2 K||_2$. Since $||\Delta^2 K||_1$ is larger than $||\Delta^2 K||_2$, the coefficient of $||\Delta^2 K||_1$ is relatively small. We obtain improved RMSEs of 1.14 mm and 3.28 ps in position and time by optimizing the joint objective function, as depicted in Fig. 3(c). The reconstructed refractive index is 1.448. The reconstruction accuracy is significantly improved because the L_1 norm preserves large curvature changes in the reconstructed path, while the L_2 norm retains the smoothness and details. Adjusting the objection function according to the characteristics of the target light paths yields better reconstruction results.

The experimental setup for 5D imaging of light propagation in a curved optical fiber is depicted in Fig. 4(a). A laser source (PicoQuant, LDH-P-635, repetition rate 20 MHz, wavelength 636 - 638 nm, 1.2 mW, pulse width 68 ps) emits laser pulses which are coupled into a multimode optical fiber with a core diameter of 50 μm. The SPAD camera is comprised of an SPAD array (Photon Force PF32, pixel resolution 32 × 32, temporal resolution 55 ps, pixel pitch 50 μm, fill factor 1.5 %) and a camera lens (Thorlabs, MVL4WA, effective focal length 3.5 mm, F/1.4). The object distance is 370 mm, where the FOV of the SPAD camera is 140 × 140 mm. The SPAD detectors, organized in a 32 × 32 array, operate independently in time-correlated single photon counting (TCSPC) mode and are synchronized to the pulsed laser. To achieve adequate photon counts, we capture 10^6 frames to form a temporal histogram, and the exposure time of each frame is 50 μs. Before data processing, a reference histogram is acquired with the laser source deactivated, and the ambient light and dark counts can be suppressed by subtracting this reference histogram.

To determine the 3D (x', y', t') data, we apply Gaussian fitting to the histograms. Efficient pixels directly detect scattered photons from the object points, resulting in significantly higher peak photon counts in their histograms. Hence, the efficient pixels can be identified by setting a proper threshold on peak counts, as illustrated in Fig. 4(b). Subsequently, the 2D (x', y') data are obtained. Additionally, we can estimate t' by the peak position of the fitted Gaussian function. Furthermore, the systematic temporal delay in each pixel is removed by adding a temporal offset. The offset value is calculated by measuring the temporal deviation between the measured peak position and the theoretical value when an expanded pulsed laser illuminates the camera. The calibrated t' is depicted in Fig. 4(c).

Since determining the ground truth of an arbitrary curved path is difficult, we attach the fiber to acrylic cylinders, forming an S-shaped curve. The diameter of the acrylic cylinder is 100 mm, providing a reference for determining the ground truth. Due to the limited pixel count and the low fill factor of the SPAD camera, the 2D (x', y') data are not the precise representation of the actual light path in real space. To

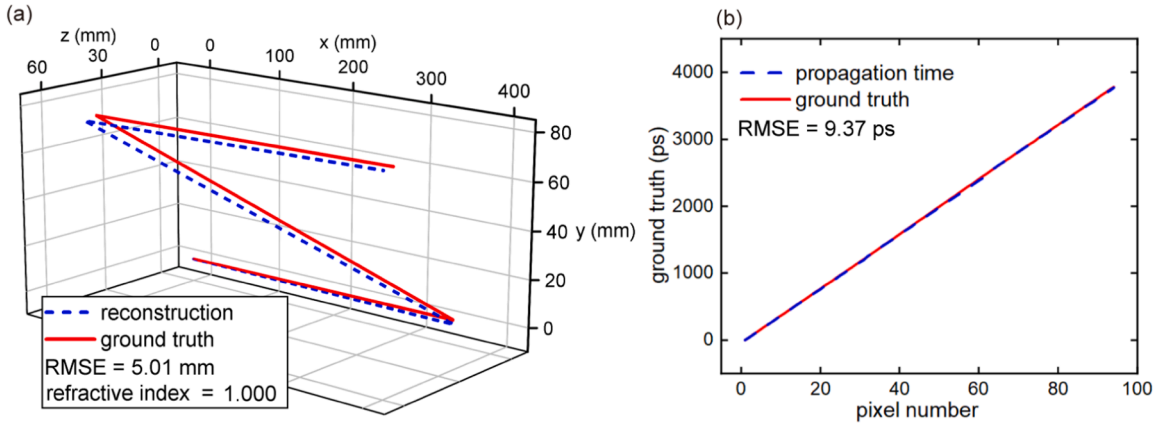

Fig. 2. The 5D imaging result of light reflecting between two mirrors in air. (a) The light path is reconstructed with a RMSE of 5.01 mm. The reconstructed refractive index of air is 1.000, and the ground truth is 1.00027. (b) The RMSE of the reconstructed propagation time is 9.37 ps.

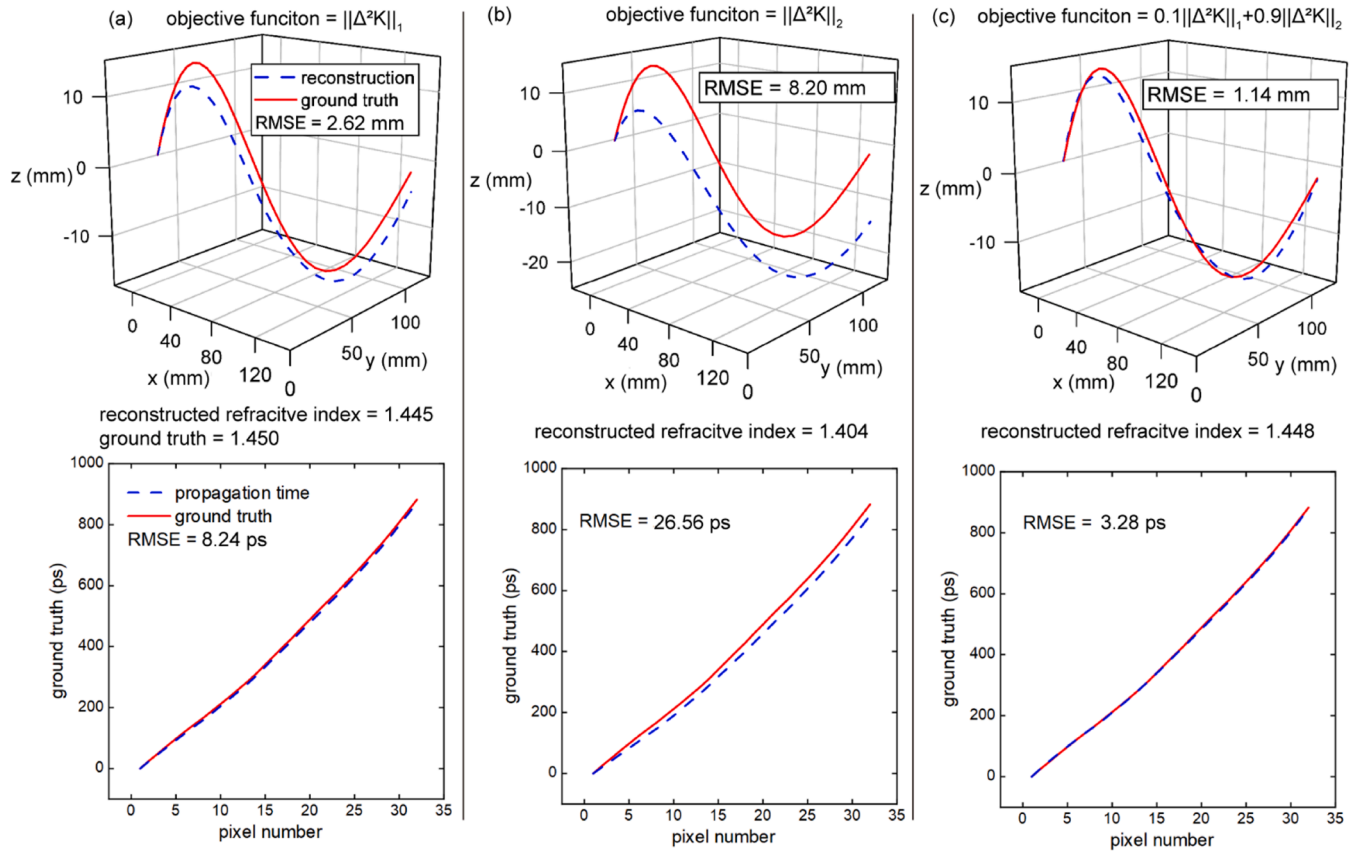

Fig. 3. Simulation results of 5D imaging when light propagates in a curved optical fiber via different objective functions. (a) The result obtained by optimizing $||\Delta^2 K||_1$. The RMSEs are 2.62 mm and 8.24 ps in position and time, respectively. The reconstructed refractive index is 1.445, while the ground truth is 1.450. (b) The result obtained by optimizing $||\Delta^2 K||_2$. The RMSEs are 8.20 mm and 26.56 ps. The reconstructed refractive index is 1.404. (c) The result obtained by optimizing a joint objective function which combines $||\Delta^2 K||_1$ and $||\Delta^2 K||_2$. The RMSEs are 1.14 mm and 3.28 ps. The reconstructed refractive index is 1.448.

avoid this impact, we present a simplified scenario where the S-shaped fiber lies in the *x*-*z* plane. This configuration guarantees that the optical fiber is captured by a single row of pixels on the SPAD array, resulting in an accurate position measurement in the *x*-*y* plane. There are 32 object points on the curved fiber.

The 5D imaging result of the S-shaped light path is shown in Fig. 5 and Supplementary Video 1, which is obtained by optimizing $||\Delta^2 K||_1$. Fig. 5(a) is a photograph of the curved fiber captured under experimental conditions using a commercial camera, where the scattered light is too weak to be detected. The reconstructed light path overlaps on the photograph, providing an intuitive reconstruction result. We take another photograph under higher laser power to display the ground truth, as depicted in Fig. 5(b).

The reconstructed path and the propagation time are illustrated in Figs. 5(c) and 5(d). The curved light path is reconstructed with a RMSE of 1.51 mm, and the RMSE of the propagation time is 3.50 ps. In data processing, we apply Gaussian fitting on multiple discrete time bins for better temporal estimation. Besides, the proposed retrieval algorithm suppresses random temporal noise. Therefore, although the original temporal resolution of the SPAD camera is 55 ps, the temporal accuracy of the result is significantly improved. The estimated refractive index of the optical fiber is 1.452, while the ground truth is 1.460. From the camera's perspective, the light path appears as a horizontal line, but we can retrieve the hidden information of depth and the refractive index via the proposed method.

We also conducted an experiment of light propagating in an optical fiber with a full 3D shape. Since the light path is a simple arc, we use $||\Delta^2 K||_2$ as the objective function. Figs. 6(c)- 6(e) quantitatively illustrate the reconstruction of the full 3D light path with a RMSE of 2.24 mm. The RMSE of propagation time is 9.49 ps, as illustrated in Fig. 6(f). The estimated refractive index of the optical fiber is 1.453.

The error in the reconstruction primarily arises from the temporal noise and the inaccurate position measurement in the *x*-*y* plane due to the low fill factor and pixel count. When reconstructing the S-shaped path, we mitigate the error in position estimation by constraining the light path in a horizontal plane. Thus, even though the full 3D path is a simple arc, its reconstruction accuracy is worse than that of the S-shape path. Employing an SPAD camera with higher pixel count and higher fill factor can improve the reconstruction accuracy for full 3D light paths.

3.3. Results of light propagating in a GRIN medium

A 5D imaging simulation of light propagating in a GRIN medium is performed. The GRIN medium has a non-uniform refractive index distribution ranging from 1.300 to 1.500 along the *z*-axis. In the simulation, the object distance is 1 m, where the FOV is 400 mm × 400 mm. The virtual SPAD camera comprises a 32 × 32 array, resulting in 32 object points and 31 layers. Since the propagation angle of light changes gradually in GRIN media, we reconstruct the light path by optimizing $||\Delta^2 K||_2$. Figs. 7(a) and 7(b) depict the reconstructed path and propagation time. The position RMSE is 0.24 mm, and the time RMSE is 0.95 ps. Fig. 7(c) illustrates the reconstructed index profile. The reconstructed refractive index agrees with the ground truth, except for the 0 mm - 30 mm range along the *z*-axis.

According to Snell's law, the refractive index of each layer is mathematically equivalent to the propagation angle of the light path segment within it. We can also use the slopes (K) of the light path segments to represent the propagation angle. Thus, the refractive index profile is

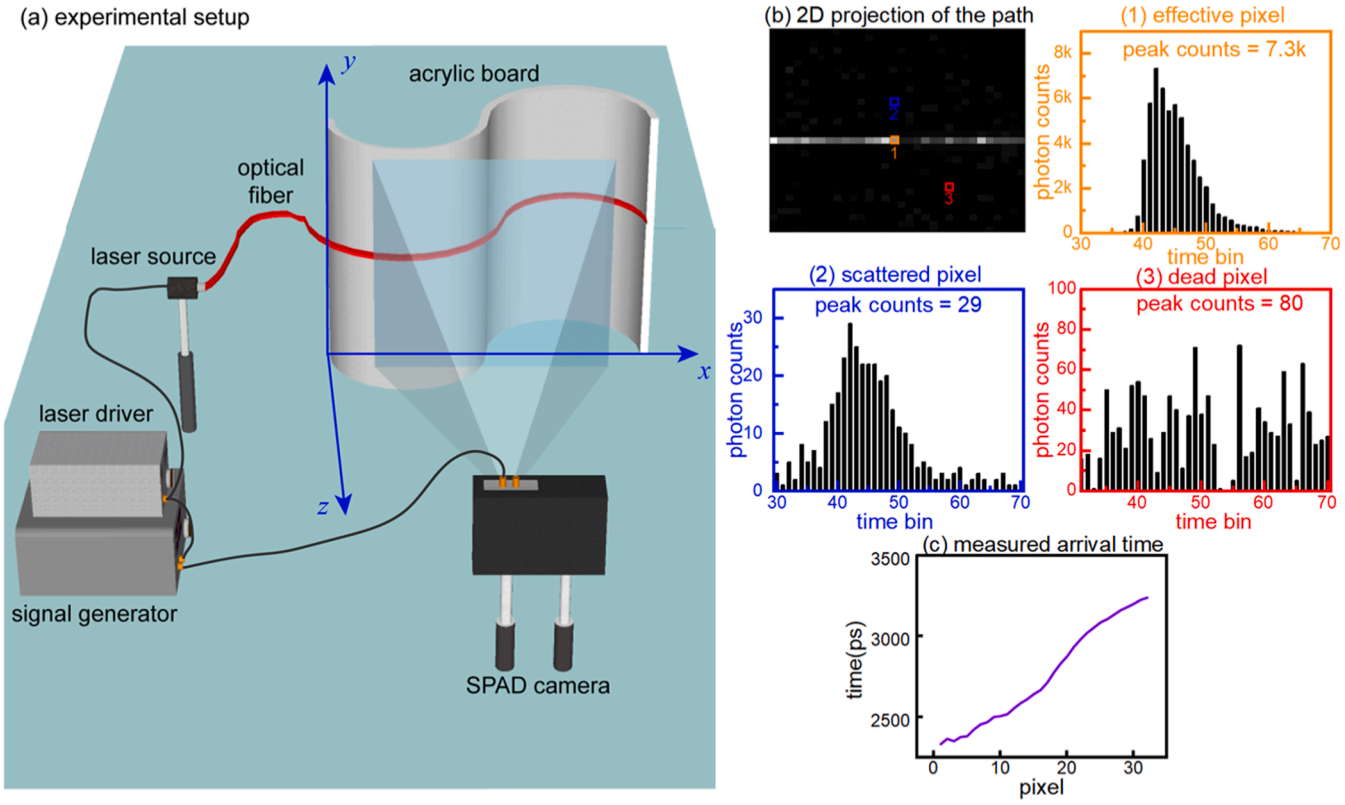

Fig. 4. The experimental setup and the data processing. (a) The schematic of the experimental setup. The pulsed laser source is synchronized to the SPAD camera, and the optical fiber is fixed on an acrylic board to form a curved path. (b) The efficient pixels with high peak counts can be distinguished by setting a proper threshold. Scattered pixels detect the scattered light from the acrylic board. The pixels with high dark counts are called "dead pixels", and the average photon counts are high even after background substruction. (c) Gaussian fitting is applied to the efficient histograms, and the peak position of the fitted Gaussian curve estimates t'.

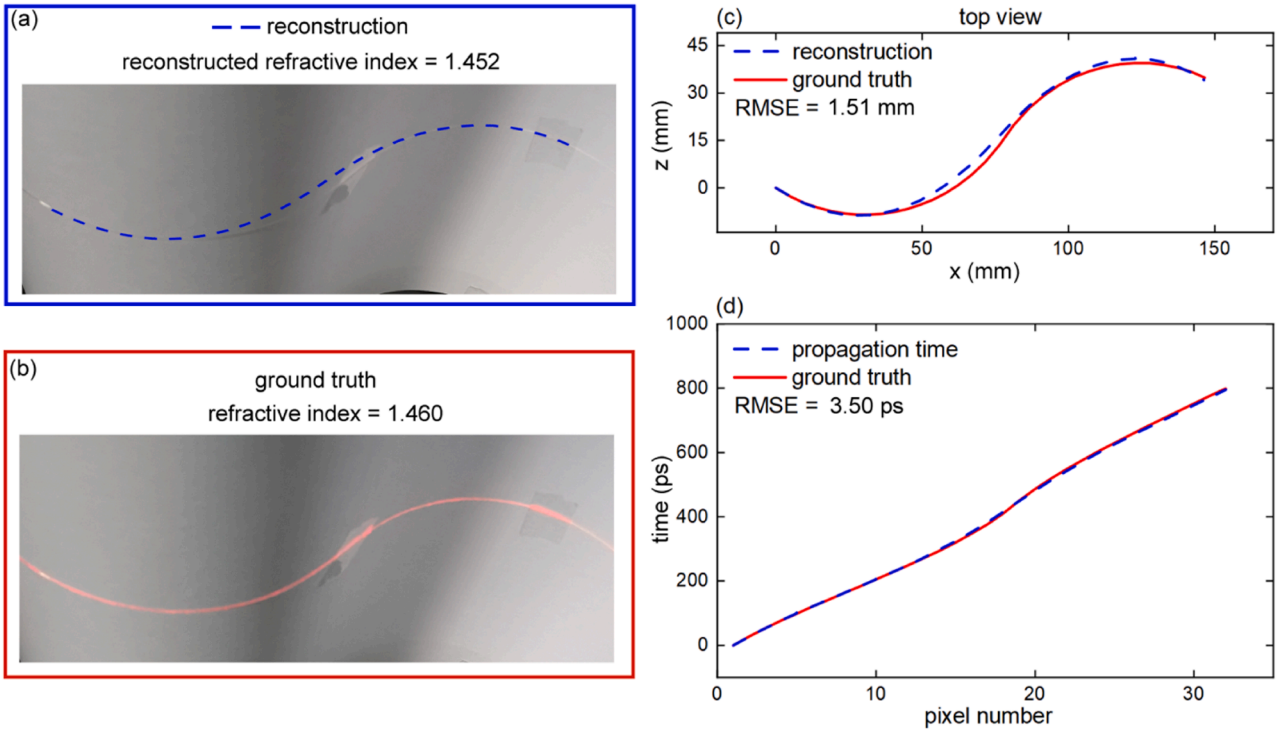

Fig. 5. The 5D imaging result of light propagating in an S-shape curved optical fiber within the x-z plane. The result is obtained by optimizing $||\Delta^2 K||_1$. (a) A photograph of the curved optical fiber captured by a commercial camera in experimental conditions, where the scattered light is too weak to be detected. The photograph is overlaid by the reconstructed path. The reconstructed refractive index of the optical fiber is 1.452, while the ground truth is 1.460. (b) A photograph captured with higher laser power. (c) The RMSE of the reconstructed curved path is 1.51 mm. (d) The RMSE of the reconstructed propagation time is 3.50 ps.

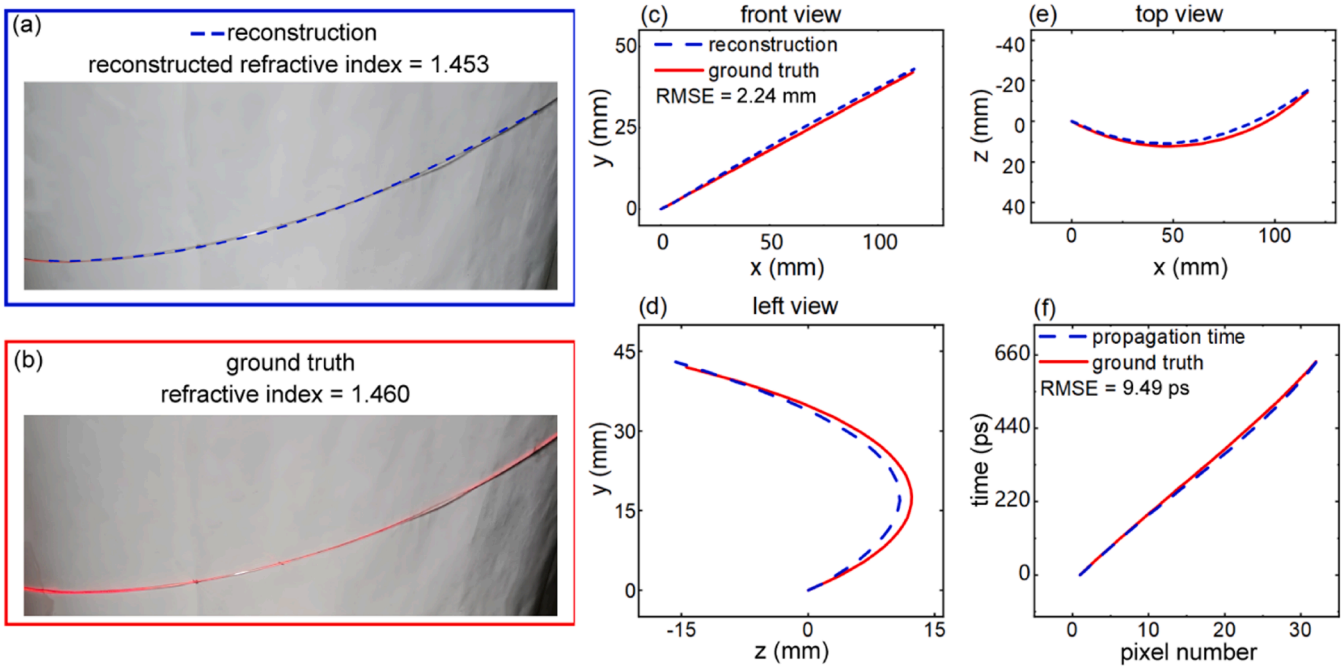

Fig. 6. The 5D imaging result of light propagating in a curved optical fiber with a full 3D shape. The result is obtained by optimizing $||\Delta^2 K||_2$. (a) A photograph of the curved optical fiber overlaid by the reconstruction result. The reconstructed refractive index of the optical fiber is 1.453. (b) A photograph of the optical fiber captured with higher laser power. (c) - (e) The quantitative path reconstruction is presented in the form of three-view drawings, and the RMSE is 2.24 mm. (f) The RMSE of the reconstructed propagation time is 9.49 ps.

intrinsically equivalent to K, which is the first-order derivative of the light path. The original objective function $||\Delta^2 K||_2$ is designed to retrieve a smooth light path. Hence, we optimize $||\Delta^3 K||_2$ to reconstruct a smooth refractive index profile. The 5D imaging result acquired by optimizing $||\Delta^3 K||_2$ is presented in Figs. 7(d)- 7(f). This result exhibits better agreement with the ground truth, and the RMSEs of position and time are 0.23 mm and 0.73 ps. Additionally, the RMSE of the refractive index improves to 0.003.

We conduct a 5D imaging experiment of light propagating within a GRIN medium composed of glycerin-water solution. The medium's dimensions are 460 × 100 × 100 mm, and it is contained in a water tank, as illustrated in Fig. 8(a). The GRIN medium exhibits a gradually increasing glycerin concentration from the top to the bottom of the tank, forming a gradient refractive index distribution along the z-axis. Both the refractive index and the density of the glycerin-water solution are proportional to the concentration, and the index distribution is quasi-static. The SPAD camera is positioned at a height of 1 m, capturing images from top to bottom. The spatial resolution of the SPAD camera is 32×32, resulting in 32 object points and 31 layers.

Before the experiment, the light enters the medium and forms a curved light path within the x-z plane due to refraction. A calibrated CMOS camera captures an image of the curved light path from the y-direction, and we calculate the coordinates of the light path in the x-z plane by the intrinsic matrix. The position measurement accuracy of the monocular system is about 0.1 mm, and we regard its measurement as the ground truth of the light path position. According to Snell's law, the shape of the light path in a GRIN medium is determined by the refractive index distribution. Therefore, we can inversely calculate the index distribution based on the measured light path and regard the calculation result as the ground truth.

The 5D imaging results of light propagating in the GRIN medium obtained by optimizing $||\Delta^3 K||_2$ are illustrated in Figs. 8(b)- 8(f) and Supplementary Video 1. The RMSE in position is 1.52 mm, and the RMSE in propagation time is 3.65 ps. The reconstructed refractive index profile is depicted in Fig. 8(e) with a RMSE of 0.003. Within the range of 60 mm to 90 mm along the z-axis, the reconstructed refractive index profile closely matches the ground truth, but notable error exists in other regions. As the process of retrieving the refractive index from t' is nonlinear, even minor errors in t' can lead to significant deviation in the refractive index profile. Therefore, an accurate measurement of the temporal data t' are the key to obtaining a good reconstruction of the refractive index. This experiment demonstrates the potential of the proposed method for non-destructively measuring the spatial distribution of light-related physical parameters.

4. Discussion and conclusion

The proposed method discretely retrieves the 4D LiF information by sampling multiple object points on the light path. According to the Nyquist-Shannon sampling theorem [25], the original signal can be retrieved when the sampling frequency is twice the frequency of a signal. Consequently, for complex light paths, we need more object points. The 32 × 32 SPAD array limits the number of object points, and we merely retrieve light paths with simple shapes. Canon Inc. has presented a megapixel SPAD camera [26], which yields higher spatial sampling frequency and enables the reconstruction of complex light paths. For a full 3D light path, the low fill factor of the SPAD pixels leads to inaccurate measurement of the (x', y', t') data, as the light path may cut across the gap between two pixels. Using an SPAD array with a high fill factor of 61 % [27], we can detect more scattered photons and measure the 3D data more accurately. Moreover, using SPAD cameras with high-resolution TDCs [28,29], we can detect finer variation in depth and refractive index.

In summary, we introduce a computational imaging method to retrieve the 5D (x, y, z, t, n) information from the 3D (x', y', t') data recorded by an SPAD camera. By discretizing both the light path and the medium, we present an optical model for projecting the 5D information to the 3D data. Subsequently, by leveraging the continuous nature of light paths, we retrieve the 5D information from the 3D data via an optimization problem. We validate the proposed method in scenarios of light propagating in a homogeneous medium, light traveling in curved waveguides, and light bending in a GRIN medium, achieving millimeter-

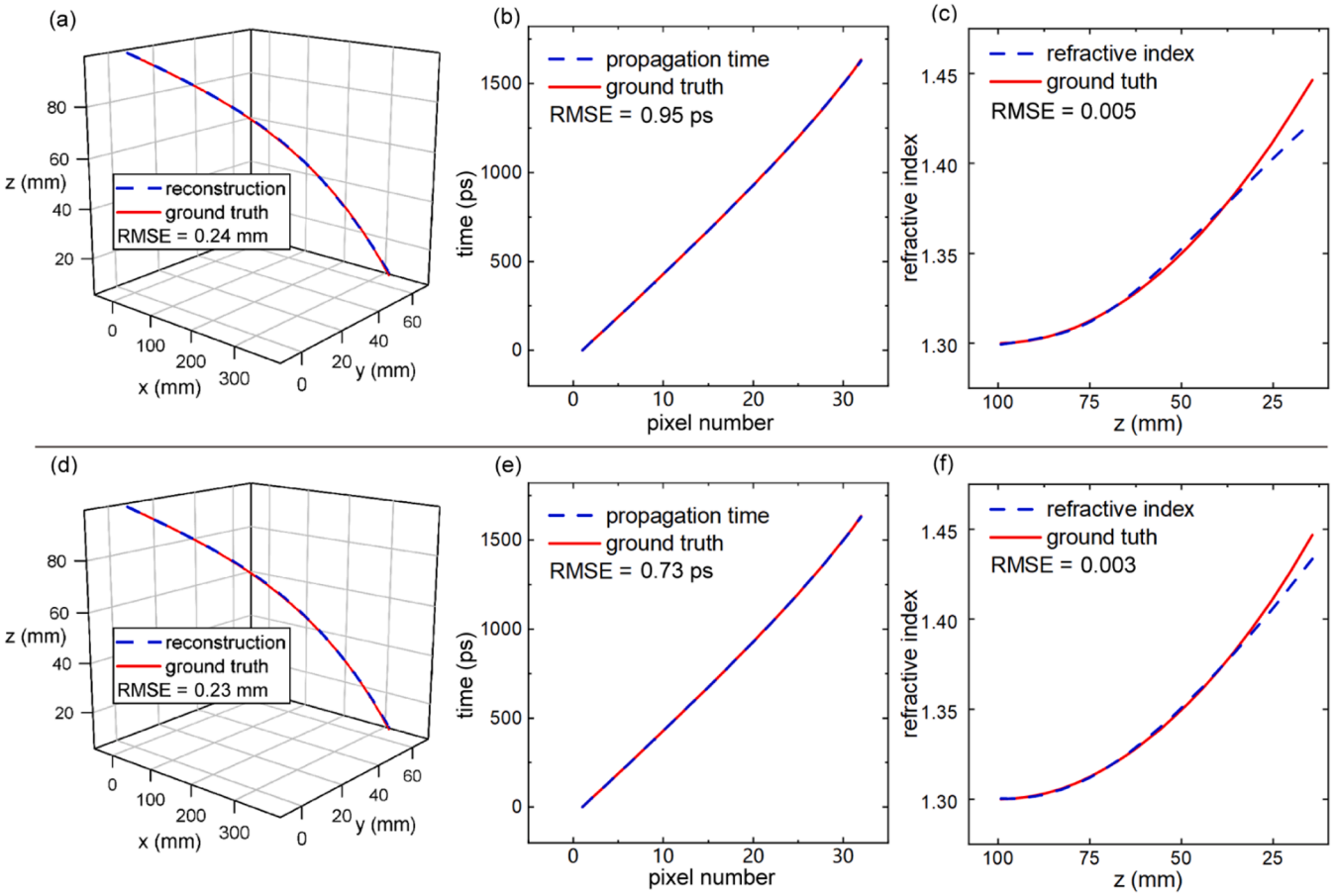

Fig. 7. The simulation result of 5D imaging in an axial GRIN medium with non-uniform index distribution. (a) - (c) The 5D imaging result acquired by optimizing $||\Delta^2 K||_2$. The RMSEs in position and time are 0.24 mm and 0.95 ps. The RMSE of the refractive index profile is 0.005. (d) - (f) The 5D imaging result acquired by optimizing $||\Delta^3 K||_2$. The RMSEs are 0.23 mm and 0.73 ps. There is better agreement between the reconstructed index profile and the ground truth, and the RMSE improves to 0.003.

level accuracy in the spatial domain and picosecond-level accuracy in the temporal domain. Additionally, the average error in refractive index measurement is approximately 0.5 %.

Although our experiments are conducted under specific conditions of light propagation, theoretically, the proposed method is effective under any scenarios involved in the general optical model (e.g., light propagates in an optical fiber embedded in a GRIN medium). We intend to explore these conditions in future research.

The proposed method broadens the application scope of LiF imaging systems based on SPAD cameras without hardware modification. Moreover, the ability to measure the refractive index provides a non-destructive way to characterize the index distribution of GRIN optical elements [30]. Other physical parameters of optical media, such as transmittance, may also be measured. We may also trace high-energy particles in electromagnetic fields by using the same imaging system, as particles have similar characteristics to photons. This work also potentially enables visualizing deep internal anatomy [31], such as delineating arterial shapes via scattered photons.

Funding

This work was supported by National Natural Science Foundation of China (U21B2034) and Open Research Projects of KLOMT (2022KLOMT02-02).

Disclosures

The authors declare no conflicts of interest.

CRediT authorship contribution statement

Zhi-Guan Wang: Conceptualization, Formal analysis, Investigation, Methodology, Writing – original draft, Writing – review & editing. **Ming-Jie Sun:** Conceptualization, Formal analysis, Funding acquisition, Methodology, Writing – original draft, Writing – review & editing. **Daniele Faccio:** Conceptualization, Formal analysis, Writing – review & editing.

Declaration of competing interest

The authors declare that they have no known competing financial interests or personal relationships that could have appeared to influence the work reported in this paper.

Data availability

Data will be made available on request.

Supplementary materials

Supplementary material associated with this article can be found, in

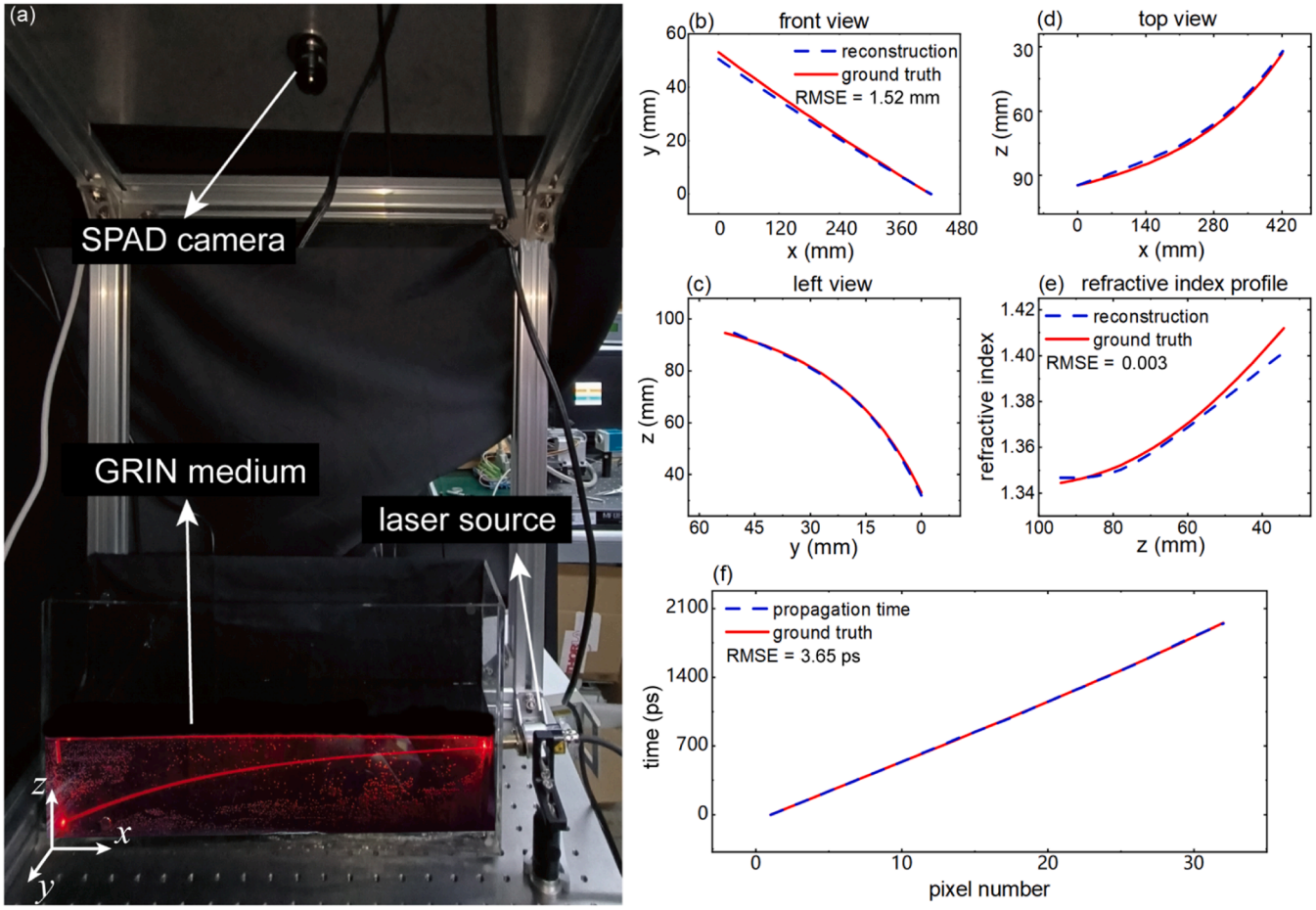

Fig. 8. The 5D imaging experiment of light propagating in a GRIN medium consisting of glycerin-water solution. (a) A photograph of the experimental setup. (b) - (d) The three-view drawings of the reconstructed light path, and the RMSE in position is 1.52 mm. (e) The reconstructed refractive index profile with RMSE of 0.003. (f) The RMSE of the reconstructed propagation time is 3.65 ps.

the online version, at doi:10.1016/j.optlaseng.2024.108088.

References

[1] Gao L, Liang J, Li C, Wang LV. Single-shot compressed ultrafast photography at one hundred billion frames per second. Nature 2014;516:74–7. https://doi.org/10.1038/nature14005.

[2] Gorkhover T, Schorb S, Coffee R, Adolph M, Foucar L, Rupp D, et al. Femtosecond and nanometre visualization of structural dynamics in superheated nanoparticles. Nat Photonics 2016;10:93–7. https://doi.org/10.1038/nphoton.2015.264.

[3] Goda K, Tsia KK, Jalali B. Serial time-encoded amplified imaging for real-time observation of fast dynamic phenomena. Nature 2009;458:1145–9. https://doi.org/10.1038/nature07980.

[4] Liang J, Wang LV. Single-shot ultrafast optical imaging. Optica 2018;5:1113–27. https://doi.org/10.1364/OPTICA.5.001113.

[5] Abramson N. Light-in-flight recording by holography. Opt Lett 1978;3:121–3. https://doi.org/10.1364/OL.3.000121.

[6] Häusler G, Herrmann JM, Kummer R, Lindner MW. Observation of light propagation in volume scatterers with 10^{11}-fold slow motion. Opt Lett 1996;21:1087–9. https://doi.org/10.1364/OL.21.001087.

[7] Kubota T, Komai K, Yamagiwa M, Awatsuji Y. Moving picture recording and observation of three-dimensional image of femtosecond light pulse propagation. Opt Express 2007;15:14348–54. https://doi.org/10.1364/OE.15.014348.

[8] Kakue T, Tosa K, Yuasa J, Tahara T, Awatsuji Y, Nishio K, et al. Digital light-in-flight recording by holography by use of a femtosecond pulsed laser. IEEE J Sel Top Quantum Electron 2012;18:479–85. https://doi.org/10.1109/JSTQE.2011.2147281.

[9] Itatani J, Quéré F, Yudin GL, MYu Ivanov, Krausz F, Corkum PB. Attosecond streak camera. Phys Rev Lett 2002;88:173903. https://doi.org/10.1103/PhysRevLett.88.173903.

[10] Heide F, Hullin MB, Gregson J, Heidrich W. Low-budget transient imaging using photonic mixer devices. ACM Trans Graph 2013;32. https://doi.org/10.1145/2461912.2461945. 45:1–45:10.

[11] Richardson J, Walker R, Grant L, Stoppa D, Borghetti F, Charbon E, et al. A 32×32 50ps resolution 10 bit time to digital converter array in 130nm CMOS for time correlated imaging. In: 2009 IEEE Cust. Integr. Circuits Conf.; 2009. p. 77–80. https://doi.org/10.1109/CICC.2009.5280890.

[12] Warburton R, Aniculaesei C, Clerici M, Altmann Y, Gariepy G, McCracken R, et al. Observation of laser pulse propagation in optical fibers with a SPAD camera. Sci Rep 2017;7:43302. https://doi.org/10.1038/srep43302.

[13] Gariepy G, Krstajić N, Henderson R, Li C, Thomson RR, Buller GS, et al. Single-photon sensitive light-in-fight imaging. Nat Commun 2015;6:6021. https://doi.org/10.1038/ncomms7021.

[14] Laurenzis M, Klein J, Bacher E. Relativistic effects in imaging of light in flight with arbitrary paths. Opt Lett 2016;41:2001–4. https://doi.org/10.1364/OL.41.002001.

[15] Zheng Y, Sun M-J, Wang Z-G, Faccio D. Computational 4D imaging of light-in-flight with relativistic effects. Photonics Res 2020;8:1072–8. https://doi.org/10.1364/PRJ.390417.

[16] Morland I, Zhu F, Martín GM, Gyongy I, Leach J. Intensity-corrected 4D light-in-flight imaging. Opt Express 2021;29:22504–16. https://doi.org/10.1364/OE.425930.

[17] Morimoto K, Wu M-L, Ardelean A, Charbon E. Superluminal motion-assisted four-dimensional light-in-flight imaging. Phys Rev X 2021;11:011005. https://doi.org/10.1103/PhysRevX.11.011005.

[18] Canfield BK, Kwiatkowski CS, Kuzyk MG. Direct deflection method for determining refractive-index profiles of polymer optical fiber preforms. Appl Opt 2002;41:3404. https://doi.org/10.1364/AO.41.003404.

[19] Nihei E, Shimizu S. Determination of the refractive index profile of polymer optical fiber preform by the transverse ray tracing method. Opt Commun 2007;275:14–21. https://doi.org/10.1016/j.optcom.2007.03.007.

[20] Zhang Z, Zhang B, Yuan X, Zheng S, Su X, Suo J, et al. From compressive sampling to compressive tasking: retrieving semantics in compressed domain with low bandwidth. PhotoniX 2022;3:19. https://doi.org/10.1186/s43074-022-00065-1.

[21] Wang Y. Smoothing spline models with correlated random errors. J Am Stat Assoc 1998;93:341–8. https://doi.org/10.1080/01621459.1998.10474115.

[22] Birch KP, Downs MJ. An updated edlén equation for the refractive index of air. Metrologia 1993;30:155. https://doi.org/10.1088/0026-1394/30/3/004.

[23] Shah P, Khankhoje UK, Moghaddam M. Inverse scattering using a joint L1-L2 norm-based regularization. IEEE Trans Antennas Propag 2016;64:1373–84. https://doi.org/10.1109/TAP.2016.2529641.

[24] Zhu Q, Zhang D, Sun H, Li Z. Combining L1-norm and L2-norm based sparse representations for face recognition. Optik 2015;126:719–24. https://doi.org/10.1016/j.ijleo.2015.02.020.
[25] Jerri AJ. The Shannon sampling theorem—Its various extensions and applications: a tutorial review. Proc IEEE 1977;65:1565–96. https://doi.org/10.1109/PROC.1977.10771.
[26] Morimoto K, Ardelean A, Wu M-L, Ulku AC, Antolovic IM, Bruschini C, et al. Megapixel time-gated SPAD image sensor for 2D and 3D imaging applications. Optica 2020;7:346. https://doi.org/10.1364/OPTICA.386574.
[27] Gyongy I, Calder N, Davies A, Dutton NAW, Duncan RR, Rickman C, et al. A 256×256, 100-kfps, 61% Fill-Factor SPAD image sensor for time-resolved microscopy applications. IEEE Trans Electron Devices 2018;65:547–54. https://doi.org/10.1109/TED.2017.2779790.
[28] Gramuglia F, Wu M-L, Bruschini C, Lee M-J, Charbon E. A low-noise CMOS SPAD pixel with 12.1 Ps SPTR and 3 Ns dead time. IEEE J Sel Top Quantum Electron 2022;28:1–9. https://doi.org/10.1109/JSTQE.2021.3088216.
[29] Korzh B, Zhao Q-Y, Allmaras JP, Frasca S, Autry TM, Bersin EA, et al. Demonstration of sub-3ps temporal resolution with a superconducting nanowire single-photon detector. Nat Photonics 2020;14:250–5. https://doi.org/10.1038/s41566-020-0589-x.
[30] Porte X, Dinc NU, Moughames J, Panusa G, Juliano C, Kadic M, et al. Direct (3+1) D laser writing of graded-index optical elements. Optica 2021;8:1281–7. https://doi.org/10.1364/OPTICA.433475.
[31] Tanner MG, Choudhary TR, Craven TH, Mills B, Bradley M, Henderson RK, et al. Ballistic and snake photon imaging for locating optical endomicroscopy fibres. Biomed Opt Express 2017;8:4077–95. https://doi.org/10.1364/BOE.8.004077.